Origin of Multiple Melting Endotherms in a High Hard Block Content Polyurethane. 2. Structural Investigation

A. Saiani,[*,†,‡] C. Rochas,[§] G. Eeckhaut,[⊥,∥] W. A. Daunch,[⊥,⊗] J.-W. Leenslag,[⊥,○] and J. S. Higgins[#]

Laboratoire de Thermodynamique des Solutions et des Polymères, Université Blaise Pascal/CNRS UMR 6003, 24, avenue des Landais, 63177 Aubière Cedex, France 1, Laboratoire de Spectrométrie Physique, CNRS UMR 5588, Université Joseph Fourier, Grenoble, B.P. 87, 38402 St. Martin d'Hères, France, Huntsman Polyurethanes, Everslaan 45, 3078 Everberg, Belgium, and Department of Chemical Engineering, Imperial College, Prince Consort Road, London SW7 2BY, U.K.

Received May 10, 2003; Revised Manuscript Received September 29, 2003

ABSTRACT: The structure and morphology of a set of high hard block content (50% to 100% hard segment by weight) linear thermoplastic polyurethanes has been investigated mainly via small angle X-ray scattering (SAXS) and transmission electron microscopy (TEM). All the results obtained in this investigation have been correlated to our previous work on the thermodynamic properties of the same set of samples (Saiani et al. *Macromolecules* **2001**, *34*, 9059). The soft segment was based on a poly(propylene oxide) polyol end-capped with ethylene oxide and the hard segment on a 4,4′-methylenediphenyleneisocyanate (MDI) chain extended by 2-methyl-1,3-propanediol (MP−Diol). Samples with a hard segment volume fraction higher than 65% are shown to have a morphology consisting in soft phase domains embedded in a hard phase matrix. Alignment of the soft phase domains could be observed under specific preparation conditions. From our SAXS results, the same average interdomain distance was found for all the samples ($d_i \approx 15$ nm). These results confirm our DSC results and suggest a two-phase structure for the melt-quenched samples: "pure" hard segment phase + mixed phase (soft + hard segments) with a hard segment content of 65 wt %. The mixed phase then undergoes phase separation during the annealing at 120 °C. The dynamics of the phase separation was also investigated showing a strong correlation between the peak observed in the scattering curves and the so-called T_{MMT} melting endotherm. The results confirm the assignment of this endotherm to the microphase mixing of the soft and hard segments. The rate of phase separation was found to be a function of the hard segment content of the samples, and a delay time was found before the start of the phase separation process for the high hard block content samples. The degree of phase separation was calculated and found to be the same for all the samples except the PU-50%HS sample, which showed a higher degree of phase separation. The interface thickness is found to increase with increasing hard segment content.

Introduction

Thermoplastic polyurethanes (TPU) are linear block copolymers typically constructed of statistically alternating soft (SS) and hard (HS) segments. Because of their numerous industrial applications, these materials have received considerable attention. Many characterization techniques have been used to try to understand the relationship between chemical architectures, morphologies, and mechanical properties of TPUs.[1,2] Their versatile physical properties are usually attributed to their microphase-separated structure deriving from the thermodynamic incompatibility between the soft and hard segments.

One important and intriguing feature of many commercial aromatic MDI/1,4-butanediol (BDO) based TPUs is the apparent multiple melting endotherms observed via differential scanning calorimetry (DSC).[3−7] We have recently reported on the thermodynamic investigation of a set of model linear TPUs with a relatively high content of hard segments: from 50 to 100 wt %. The soft segment of these samples consists of poly(propylene oxide), end-capped with ethylene oxide (PPO−EO), while the hard segment is composed of 4,4′-MDI, chain extended by a short diol chain: MP−Diol. In this previous work, the origin of the high temperature endothermic transitions was investigated using mainly DSC. The two observed high-temperature transitions were shown to be related to the melting of an ordered structure appearing during the annealing at 120 °C in the hard phase (T_M) and to the microphase mixing transition of the soft and hard segments (T_{MMT}). For more detail on the thermodynamic investigation of these samples, please see ref 8.

In this article, we report on the structural investigation of the same set of high hard block content samples. First the structure and morphology of the samples annealed at 120 °C will be investigated then the structural information obtained will be correlated to the thermodynamic behavior of the samples in order to give further support to the assignment of the so-called T_{MMT} endotherm to the microphase mixing of the soft and hard segments. This structural investigation was carried out using mainly small-angle X-ray scattering (SAXS) and transmission electron microscopy (TEM).

† Université Blaise Pascal/CNRS UMR 6003.
‡ Permanent address: Manchester Materials Science Centre, University of Manchester−UMIST, Grosvenor Street, Manchester M1 7HS, U.K. E-mail: a.saiani@umist.ac.uk.
§ Université Joseph Fourier. E-mail: Cyrille.Rochas@ujf-grenoble.fr.
⊥ Huntsman Polyurethanes.
∥ E-mail: guy_eeckhaut@huntsman.com.
⊗ Permanent address: Triangle Analytical, Inc., 481 James Jackson Avenue, Cary, NC 27513. E-mail: wad@triangleanalytical.com.
○ E-mail: jan-willem_leenslag@huntsman.com.
Imperial College. E-mail: j.higgins@ic.ac.uk.

10.1021/ma034604+ CCC: $27.50
Published on Web 01/28/2004

Table 1. Average Molecular Weights and Polydispersities in Polystyrene Equivalent of the TPU Samples

samples	hard segment vol fraction Φ_{HS}	M_w	M_n	M_w/M_n	calcd av M_w of hard segment[a]	calcd av no. of MDI per hard segment[a]
PU-50%HS	0.45	24 600	8300	3.0	3700	11
PU-65%HS	0.60	38 200	12 500	3.1	6900	20
PU-75%HS	0.71	43 200	12 500	3.5	11 100	33
PU-80%HS	0.76	69 800	12 700	5.5	14 800	44
PU-85%HS	0.82	33 400	11 300	3.0	21 000	62
PU-90%HS	0.88	55 500	13 700	4.1	33 300	98
PU-100%HS	1	44 200	11 200	4.0		131[b]

[a] Calculated from Peeble's most probable distribution.[21,22] [b] Calculated directly from the measured molecular weight (M_w).

Experimental Section

Synthesis. All polyurethane samples were based on a prepolymer formulation. First, a master batch of prepolymer was prepared by reacting 1 mol of a commercial two-functional propylene oxide (PPO) ethylene oxide (EO), EO−PPO−EO, triblock copolymer (dried Daltocel F460 from Huntsman Polyurethanes: $M_w = 3700/M_n = 3083$) with 11.2 mol of 4,4′-methylenediphenylene isocyanate (4.4′-MDI) (Suprasec from Huntsman Polyurethanes). Second, a mixture of this prepolymer and 4.4′-MDI, so as to obtain the desired weight ratio between soft and hard segments, was slowly added to a preheated (85 °C) solution in dimethylacetamide (DMAC) of 2-methyl-1,3-propanediol (MP−Diol) in the presence of 0.25% catalyst (DABCO-S from Air Products).

The polymers were then isolated by precipitation. The cold PU/DMAC solution was added dropwise to a water (80)/ethanol (20) solution. The precipitated thermoplastic polyurethanes were filtered, washed with ethanol, and dried at room temperature. The dried powders were then grounded at room temperature into smaller grains, washed for a second time with the ethanol/water mixture and finally dried in a vacuum oven at 120 °C. These TPU powders were compression molded into solid plaques at elevated temperature (160−200 °C depending on the hard segment content). A series of samples with a concentration of hard segments going from 50 to 100 wt % were synthesized. A direct reaction of the prepolymer with 2-methyl-1,3-propanediol without adding extra 4,4′-MDI gave the 50 wt % hard segment sample and for the synthesis of the 100% hard segment sample, pure Suprasec MPR was reacted with 2-methyl-1,3-propanediol in a stoichiometric ratio.

The TPU samples were stored in a desiccator under dried atmosphere until used. Samples are designated according to the following nomenclature: PU-*XX*%HS where *XX* indicates the hard segment concentration by weight of the sample.

Gel Permeation Chromatography. GPC was used to determine the molecular weights of the TPUs. A dilute solution (0.2% of polymer) was prepared in tetrahydrofuran (THF) and stirred overnight. The solutions were filtered through a 0.2 μm polyamide filter. The measurements were performed by Rapra Technology Ltd. at 30 °C using a polystyrene calibration and therefore the molecular weights are given in polystyrene equivalent. The molecular weights and polydispersities of the samples are listed in Table 1.

Small-Angle X-ray Scattering. Except for the SAXS experiment carried out on the PU-50%HS sample, all other SAXS experiments were performed on beamline BM2 at the European Synchrotron Radiation Facility (ESRF), Grenoble, France. The incident energy used was 15 keV corresponding to a wavelength of 8.3×10^{-2} nm. A collimated beam was produced with a typical cross section of 0.1×0.3 mm^2 at the sample position. Two-dimensional SAXS patterns were collected on a 2D CCD detector (ref. TECCD1242 E1FG0M) from Princeton Instruments, presently Roper Scientific (further details are available on request at Roper Scientific). The sample to detector distance was ∼1 m, corresponding to a momentum transfer vector (q) range of $0.2 < q$ (nm^{-1}) < 4.5, q being defined as $q = (4\pi/\lambda) \sin(\theta/2)$, λ and θ being, respectively, the wavelength and the scattering angle (further details are available on request at the ESRF).

The samples for the SAXS experiments were prepared by cutting ∼1 cm^2 samples from the molded plates. To erase all previous thermal histories, the samples were melted at 220 °C for 2 min,[8] and then pressed at high temperature so as to achieve a sample thickness of ∼1 mm. To collect the SAXS data, the sample were placed in a 1 mm thick stainless steel holder closed by two mica windows each 25 μm thick. A home-built aluminum heating stage allowing a temperature control of ±1 °C was used for the melting and annealing experiments. The scattering intensities obtained were corrected for the detector response, the dark current, the empty cell, the sample transmission, and the sample thickness. The two-dimensional pictures were radially regrouped in order to obtain the one dimensionnal SAXS pattern. A Lupolen standard was used for the intensity normalization and a collagen sample for the momentum transfer vector, q, normalization.

For the PU-50%HS sample, the SAXS experiment was carried out at CCLRC Daresbury Laboratory, Warrington, U.K., on beamline 8.2 of the Synchrotron Radiation Source (SRS). A highly collimated beam was produced with a typical cross section of 0.3×4 mm^2 in the focal plane. An evacuated flight tube was placed between the sample and the detector in order to reduce air scattering and absorption. The SAXS data were collected on a multiwire quadrant detector with an opening angle of 70° and an active length of 0.2 m. The sample−detector distance was 3.5 m corresponding to an available momentum transfer vector range of $0.1 < q$ (nm^{-1}) < 2.0 (further details are available on request at the CCLRC). A Linkam hot stage was used allowing sample heating at a fixed rate. A heating rate of 5 °C min^{-1} was used and SAXS patterns were recorded every 10 s. The silver heating block of the Linkam hot stage contained a 4×1 mm conical hole that allowed the transmitted and scattered X-rays to pass through unhindered. The samples were prepared in the same way as described above. A ∼1 mm thick sample was then placed in a standard aluminum pan equipped with two 25 μm thick mica windows and heated with a rate of 5 °C/min. The 1D scattering intensities obtained were corrected for the detector response, the empty cell and the sample transmission. A wet rat tail collagen sample was used for the normalization of the transfer momentum vector, q.

Transmission Electron Microscopy. Scanning transmission electron microscopy (TEM) was carried out using a Philips CM20 microscope. The desired thermal treatment was applied to the sample prior to cutting. Using a Reichter-Jung ultramicrotome fitted with a glass knife, small pieces of samples where trimmed into pyramidal shapes. Sample pieces were then placed in a sealed chamber to be stained for 1 week at room temperature under an osmium tetraoxide (OsO_4) atmosphere. Finally the samples were sectioned from the top of the stained pyramid using the ultramicrotome fitted with a diamond knife. The ∼100 nm thick slices were then placed on a copper grid and examinated under the electron microscope.

Results and Discussion

Structure and Morphology. The thermal stability of our samples and the thermal protocol used to investigate them has been extensively discussed in our previous article.[8] In this earlier work, a thermal protocol was established in order to melt and anneal the samples to avoid significant degradation. The same protocol has been used for this present work. The samples were melted at 220 °C for 2 min in order to erase all previous

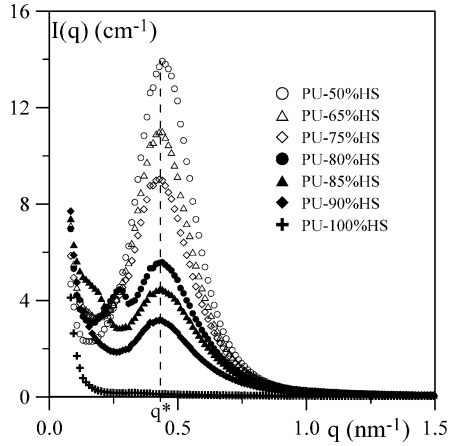

Figure 1. Intensity scattered by our set of samples after they were annealed for 72 h at 120 °C.

thermal histories and then annealed for 72 h at 120 °C, just above the glass transition of the hard segments (T_{gHS} = 119 °C). The DSC results obtained in this previous work suggested that after 72 h annealing at 120 °C the phase separation process has reached its maximum for all the samples. It indicates, as far as phase separation is concerned, that all the samples are in an equivalent thermodynamic state (i.e., maximum phase separation) and therefore can be compared.[8] For more details on the thermal protocol used, please see ref 8.

The microphase-separated morphology of TPUs depends on the fabrication and processing route as well as the molecular formulation. The size scale of the density fluctuations of the mesophase morphology is closely linked to the volume fractions as well as the characteristic molecular dimensions of the hard and soft segments. Typically the size scale is on the order of 10 nm, thus allowing the morphology to be monitored by small-angle X-ray scattering (SAXS)[1]. SAXS has been extensively used to investigate mainly low hard segment content systems.[9−13] Usually an intensity maximum characteristic of the microphase-separated morphology is observed in the scattering curve ($I(q)$ vs q). To derive quantitative mesoscopic parameters from SAXS results the knowledge (or assumption) of the microphase geometry is essential.[14−16] For the ease of interpretation of SAXS data, it is often assumed that TPUs have a lamellar mesophase structure, but this seems not to be the case for all systems,[17−21] and therefore, care should be taken when quantitative data are extracted from SAXS results. In particular, electron microscopy experiments have shown that sample preparation and sample composition can affect the morphology.[18−20] In our case, the same samples were used for the SAXS and TEM experiments.

In Figure 1 are presented the one-dimensional SAXS patterns obtained for our set of samples after melting and annealing. For all the samples an intensity maximum can be observed in the scattering curve at q^* = 0.43 nm^{-1}. For PU-80%HS and PU-85%HS samples, an additional smaller peak (shoulder) can be observed at lower q values. The origin of this second peak will be discussed later. First we will focus on the structural origin of the main scattering peak.

The hard segment volume fractions, Φ_{HS}, of our samples are listed in Table 1. It is usually expected for polyurethane systems with a hard segment volume fraction higher than 50% to have a continuous hard phase.[13] For the PU-50%HS the volume fraction is lower than 50%, and therefore, it is not clear if this sample will have the same morphology as the other samples. In this article, we will mainly focus on samples with a hard segment content higher than 65 wt %.

To check the microphase morphology of our samples we performed TEM experiments. The samples were stained using OsO_4, which preferentially stains the soft segments.[18−20] The stained areas will then appear darker on the micrographs. In Figure 2 are presented the TEM micrographs obtained for the PU-65%HS and the PU-85%HS samples. A clear microphase-separated structure can be observed for both samples in which soft phase domains (darker regions) are embedded in a continuous hard phase matrix (brighter regions). A similar morphology was observed for high hard block content polybutadiene polyurethanes.[18−20] The soft phase domains do not show a regular shape and seem to be relatively polydispersed in sizes. The PU-65%HS sample seems to have larger soft phase domains than the PU-85%HS sample. TEM pictures are two-dimensional projections of three-dimensional samples. For the PU-65%HS sample, having a larger content of soft segments, the probability of soft segment domains overlapping in the vertical direction is higher than in the PU-85%HS sample. This artifact could be at the origin of the apparently larger dark domains observed in the TEM micrographs of the PU-65%HS sample. Estimation of domain sizes from TEM pictures alone should be treated with care as they can be misleading.

As said earlier a main maximum is observed in the scattering curves for all the samples at the same q position (Figure 1). Scattering pattern for multiphase systems are a complex function of the structure and the arrangement of the different scattering phases. A rigorous interpretation of the origin of a single scattering peak in a SAXS curve can be made only for specific arrangements and structures.[14−16] In our case neither specific shape nor regular arrangement are observed for the soft phase domains (Figure 2). Therefore, only an estimated value of the average size of the density fluctuation of the observed morphology, d_i, can be obtained from the position of the peak maximum, q^*, through the Bragg relation:[14,15]

$$d_i = \frac{2\pi}{q_{max}} \tag{1}$$

d_i = 14.6 nm is obtained. d_i can be seen as a rough estimation of the average interdomain distance between soft phase domains. The average interdomain distance for a nonoriented structure can also be estimated from the analysis of the three-dimensional correlation functions $\gamma_3(r)$:[14,15]

$$\gamma_3(r) = \frac{1}{Q}\int_0^\infty q^2 I(q)\frac{\sin(qr)}{qr}\,dq \tag{2}$$

where Q is the so-called invariant (Q will be defined later in this article). As can be seen from Figure 3, the correlation functions show a periodicity suggesting that the structure is not totally random. An estimation of the average interdomain distance can be obtained from the first maximum which are found at the same position for all the samples. d_i = 15.8 nm is obtained. The values derived for d_i from the scattering curves and from the correlation functions are in good agreement. Several authors have described correlation function analysis of

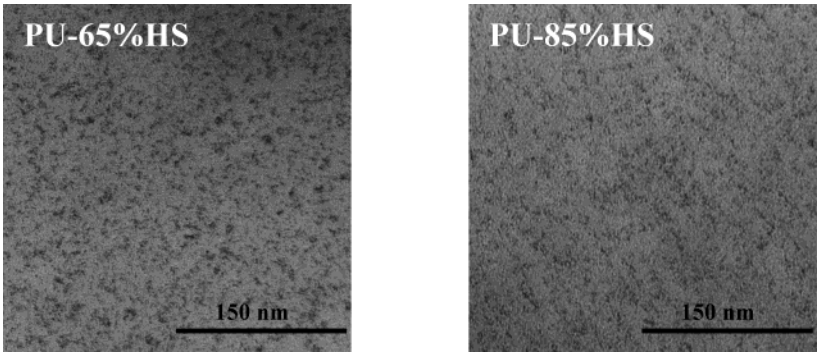

Figure 2. TEM micrographs of the PU-65%HS sample (left) and the PU-85%HS sample (right) after being annealed 72 h at 120 °C.

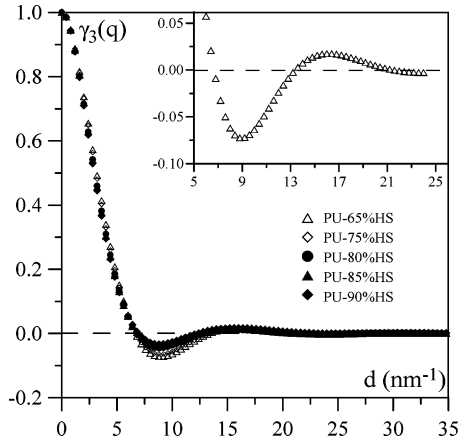

Figure 3. Three-dimensional correlation function of our set of samples after being annealed 72 h at 120 °C. Top right corner: enlargement of the correlation function obtained for the PU-65% sample.

SAXS curves.[14,15] The correlation functions obtained for our samples are reminiscent of a system having a broad distribution of interdomain distances and domain sizes and having diffuse interfaces between domains. These findings are in good agreement with the morphology observed by TEM (Figure 2).

One interesting and intriguing feature of our SAXS results is that the scattering maximum in the $I(q)$ vs q curves (Figure 1) and the first maximum position in the correlation functions (Figure 3) are found at the same positions for all the samples. This suggests that the length scale of the electron density fluctuations giving rise to the scattering maximum observed is the same for all the samples. In other words, it suggests that the microphase-separated morphology is similar for all the samples.

For the type of morphology suggested by our TEM micrographs (i.e., soft phase domain imbedded in a hard phase matrix, Figure 2), assuming that the morphology is homogeneous throughout the all volume of the samples, we would expect d_i to increase with decreasing soft segment content. Indeed, provided that the degree of phase separation is the same for all the samples, which is the case as we will see later, a diminution of the volume fraction of soft segments should result in a diminution of the average size of the soft phase domains or an increase in the average distance between soft phase domains or both of those effects. It has to be stressed again that the size, d_i, extracted from our SAXS results is an estimation of the size scale of the electron density fluctuations of the mesophase structure of the samples. Any changes in the average size of the soft phase domains or average distance between them will result in a change in the position of the maximum in the SAXS curves. We should therefore observe a shift of the intensity maximum in the scattering curves toward small q values with increasing hard segment content. This is not the case for our samples (Figure 1). It is interesting to note that in an early work by Koberstein et al. the same results were obtained for high hard block content MDI/BDO-based polyurethanes. In this work, the authors investigated samples with a hard segment content ranging from 30 to 80 wt %. For the low hard segment content samples, the scattering maximum position was found to be dependent on the hard segment content. However, for the two high hard block content samples (70 and 80 wt %), the scattering maximum was found at the same position and the same d_i of 15.1 nm was derived from the $I(q)$ vs q curve through the Bragg relation for both samples.[13] This value is in good agreement with the d_i obtained for our set of samples.

As said earlier, the samples used for our SAXS experiments were in a first stage melt-quenched (melted at 220 °C for 2 min and then quenched at room temperature) and then annealed at 120 °C for 72 h. The thermodynamic investigation of the same set of polyurethanes suggested that melt-quenched samples with a hard segment content higher than 65 wt % are not homogeneous. Our DSC results could be explained by considering the presence after melting and quenching of two phases: a "pure" hard segment phase and a mixed phase. The mixed phase was found to have a constant hard segment concentration for all the samples of 65 wt %.[8]

If this morphology is assumed, then during the annealing process at 120 °C the phase separation is expected to take place only in the mixed phase, resulting in a phase-separated mesophase. The mixed phase being the same for all the samples (i.e., same hard segment concentration 65 wt %), the morphology obtained for this phase-separated mesophase is expected to be the same. The "pure" hard segment phase being a homogeneous amorphous phase, it will not scatter; only this phase-separated mesophase will. We then expect the same length scale for the electron density fluctuations, in other words the same d_i, to be observed for all the samples. Our SAXS results seem to support this interpretation as indeed the same d_i is obtained for all our samples.

In Figure 4, diagrams A and B, a schematic illustration of the contrast mechanism implied by our structural interpretation is presented for a sample with a mixed phase volume fraction lower than 50% (i.e., 74% hard

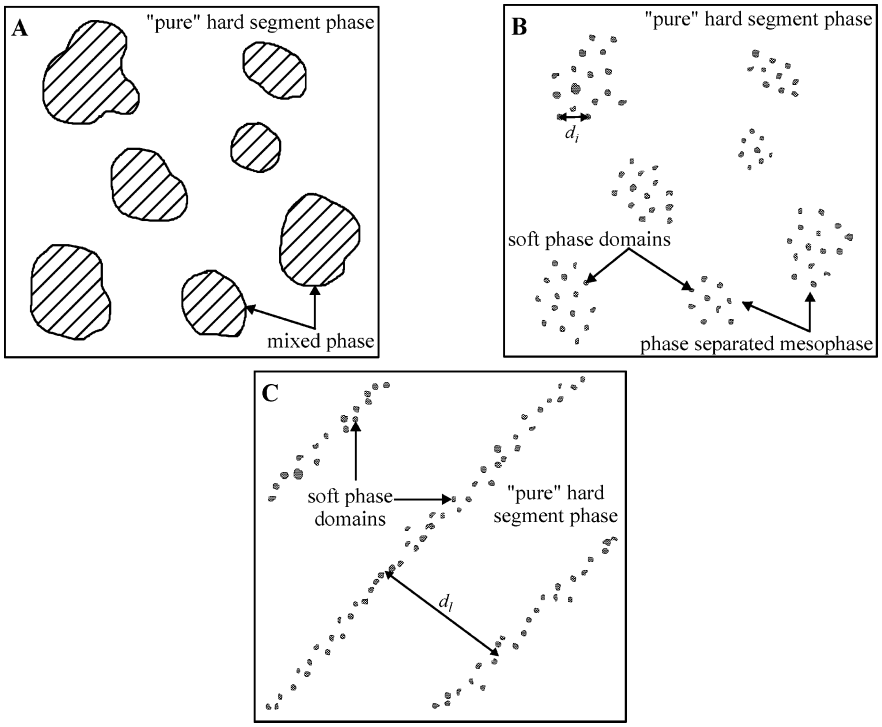

Figure 4. Schematic representation of the contrast mechanism implied by our morphological model (see text for details). (A) *Melt-quenched samples*: two phases are present, a "pure" hard segment phase and a mixed phase consisting of mixed soft and hard segments with a hard segment content of 65 wt %. (B) *Microphase-separated samples*: phase separation takes place in the mixed phase resulting in a so-called phase-separated mesophase. The scattering is due to the contrast existing between the soft phase domains and the hard phase matrix. The total scattered intensity is proportional to the volume fraction of the scattering phase, i.e., to the volume fraction of phase-separated mesophase, which is the same as the volume fraction of mixed phase in the melt-quenched samples. d_l extracted from the main scattering peak in the SAXS curves (Figure 1, see text for details) corresponds then to a rough estimation of the average interdomain distance between soft phase domains in the "phase-separated mixed phase". (C) *Sheared microphase separated samples*: when mechanical stress is applied to the sample the existing morphology is disrupted and the soft phase domains align forming a lamellar type morphology. d_l extracted from the anisotropic scattering peak at low q (see text for details) corresponds then to the lamellar repeat distance. The scattering patter in Figure 6 is the result of both morphologies B and C being present simultaneously in the sample.

segment by weight). For a sample with a mixed phase volume fraction higher than 50% the inverse picture would be expected. Nevertheless, the contrast mechanism described in Figure 4 is valid for both situations. It has to be stressed that this figure is not intended as a representation of the true sample morphology but only as a visual aid to the reader. For instance, it is not clear to us whether the mixed phase is bicontinuous or if, as depicted in Figure 4, it is formed by large mixed phase domains embedded in the "pure" hard segment phase. A specific investigation of the melt-quenched samples is underway in order to get a better understanding of their morphology.

More support for this structural interpretation is obtained from the scattering intensities. In SAXS experiments, the overall scattered intensity, I_t, is proportional to the volume fraction of the scattering phase.[14] As stated previously, the "pure" hard segment phase, being a homogeneous amorphous phase, will not contribute to I_t. Only the phase-separated mesophase will contribute to the overall scattered intensity. The volume fraction of phase-separated mesophase in the annealed samples is the same than the volume fraction of mixed phase in the melt-quenched samples. Therefore, if we assume that the degree of phase separation is the same for all the samples, then

$$I_t = \int_0^\infty I(q)\, dq \propto \Phi_{MP} \tag{3}$$

Φ_{MP} being the volume fraction of mixed phase. As stated previously, the mixed phase has the same concentration for all the samples: 65 wt % (i.e., 60% volume fraction of hard segments), and therefore, Φ_{MP} is directly proportional to the volume fraction of soft segments, Φ_{SS}, present in the sample:

$$\Phi_{MP} = \frac{\Phi_{SS}}{(1 - 0.6)} \tag{4}$$

We then expect, if our interpretation of the structure of the samples is correct, the total scattered intensity to decrease linearly with decreasing soft segment volume faction. In Figure 5 are plotted the overall scattered intensities as a function of Φ_{SS}. As can be seen the intensity is indeed decreasing linearly with decreasing Φ_{SS}, giving further support to our structural interpretation.

We now turn to the origin of the additional peak (shoulder) observed at low q for the PU-80%HS and PU-85%HS samples. In Figure 6 are presented the TEM micrograph and the corresponding two-dimensional scattering pattern obtained for the PU-80%HS sample. The TEM micrograph clearly shows the presence of areas where the soft phase domains align along parallel lines forming a lamellar type structure. As can be seen clearly on the two-dimensional scattering pattern, the peak at low q is not isotropic and therefore probably corresponds to the repeat distance between the lines on which reside the soft phase domains (Figure 4, diagram C). The repeat distance, d_l = 22 nm, obtained in this

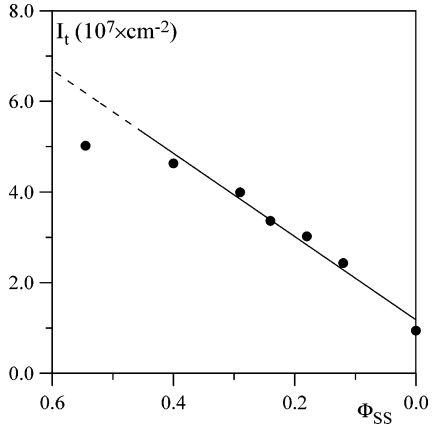

Figure 5. Total scattered intensity, I_t, as a function of soft segment volume fraction of the samples, Φ_{SS}, after being annealed for 72 h at 120 °C. The integration was limited to the experimental q range.

case from the Lorentz corrected curve $q^2I(q)$ vs q through the Bragg relation[14−16] is in good agreement with the TEM micrograph. The intensity of this peak is lower for the PU-85%HS sample, suggesting a much lower degree of alignment of the soft phase domains. Indeed, a careful examination of the micrographs of this sample (Figure 2) reveals the presence of some areas with a weak alignment of the soft phase domains. In this case the scattering maximum is found to move to smaller q values with increasing hard segment content indicating an increase of the repeat distance, d_l, between the soft phase domains lines. For the PU-85%HS sample a repeat distance of $d_l = 31$ nm is obtained. The increase of d_l is not surprising, as for a lamellar type morphology it is indeed expected for d_l to increase with increasing volume fraction of hard segments.

The alignment of the soft phase domains is due to the sample preparation method. As described in the previous section the SAXS samples were prepared by pressing the material in order to achieve a ∼1 mm thickness. Even though the pressing was carried out at high temperature, the samples were allowed to cool under pressure. The stress resulting from the compression induced the alignment of the soft phase domains resulting in a lamellar-type structure. After melting and annealing the samples again, the low q peak is no longer observed while the peak at 0.43 nm^{-1} is. This indicates that the soft phase domains do not align in the absence of mechanical stress. Shearing the samples disrupts the original morphology and induces an alignment of the soft phase domains resulting in a lamellar type morphology. This kind of behavior has already been observed for other polyurethane systems[18,19] and is relatively common for block copolymers where highly oriented lamellar phases can be obtained under shear.[22]

Alignment of the soft phase domains was not observed for the lower hard block content samples. Because of the plasticizing effect of the soft segments, the viscosity of polyurethane samples decreases with increasing soft segment concentration. The viscosity of the lower hard block content samples is probably low enough to avoid the alignment of the soft domains during the pressing at high temperature. For the PU-90%HS sample, the second scattering peak is not observed, suggesting that the sample did not align or that the peak is too low to be observed with this experimental configuration. It should be added that the degree of alignment of the soft domain is highly influenced by the temperature profile during sample preparation. For instance, highly aligned PU-85%HS samples could be obtained by pressing the sample at lower temperatures. A more detailed investigation of the effects of preparation conditions on the morphology of this set of samples is underway.

The simultaneous presence of the isotropic scattering peak at 0.43 nm^{-1} and of the non isotropic scattering peak at lower q values is simply due to the fact that the samples are not homogeneous. Some areas of the samples present an alignment of the soft phase domains while other areas do not (Figure 6). Therefore, the scattering curves obtained are a superposition of the scattering due to the two types of sample morphologies.

Degree of Phase Separation. The degree of phase separation of block copolymers can be estimated from the one-dimensional scattering pattern through the calculation of the electron density variances regardless of the type of morphology. The degree of phase separation is usually defined as the ratio[14,15]

$$\overline{\Delta\rho_e^2}/\overline{\Delta\rho_c^2} \tag{5}$$

between the experimental electron density variance

$$\overline{\Delta\rho_e^2} = \Phi_{HP}\Phi_{SP}(\rho_{HP} - \rho_{SP})^2 \tag{6}$$

Φ_{SP}, Φ_{HP}, ρ_{SP}, and ρ_{HP} being respectively the soft phase (SP) and the hard phase (HP) volume fractions and electron densities and the calculated theoretical electron density variance assuming complete phase separation

$$\overline{\Delta\rho_c^2} = \Phi_{HP}^c\Phi_{SP}^c(\rho_{HP}^c - \rho_{SP}^c)^2 \tag{7}$$

Φ_{SP}^c, Φ_{HP}^c, ρ_{SP}^c, and ρ_{HP}^c being in this case the soft phase (SP) and the hard phase (HP) volume fractions

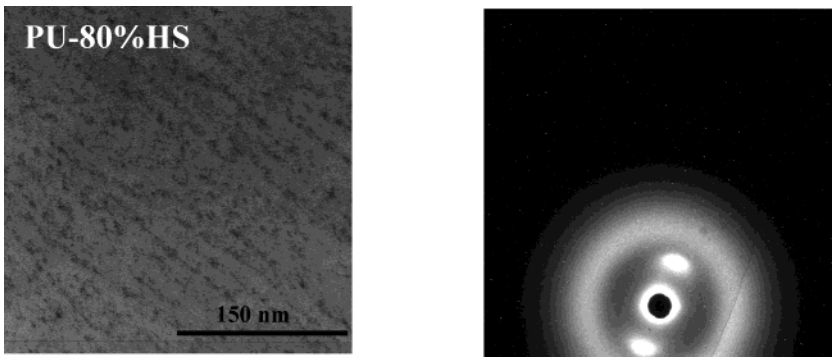

Figure 6. TEM micrographs (left) and two-dimensional scattering pattern (right) of the PU-80%HS sample after being annealed for 72 h at 120 °C.

Table 2. Calculated and Experimental Electron Variances of the TPU Samples

	sharp boundary ($E = 0$)			sigmoidal boundary ($E = \sqrt{2\pi}\sigma$)		
samples	$\overline{\Delta\rho_c^2} \times 10^3$ $(e^- \text{ mol/cm}^3)^2$	$\overline{\Delta\rho_e^2} \times 10^3$ $(e^- \text{ mol/cm}^3)^2$	phase separation (%) $\overline{\Delta\rho_e^2}/\overline{\Delta\rho_c^2} \times 100$	$\overline{\Delta\rho_e^2} \times 10^3$ $(e^- \text{ mol/cm}^3)^2$	phase separation (%) $\overline{\Delta\rho_e^2}/\overline{\Delta\rho_c^2} \times 100$	boundary thickness E (nm)
PU-50%HS	3.39	1.90	56	2.35	69	1.1
PU-65%HS	3.28	1.54	47	1.99	61	1.3
PU-75%HS	2.82	1.34	48	1.86	66	1.5
PU-80%HS	2.50	0.98	39	1.37	55	1.4
PU-85%HS	2.02	0.83	41	1.30	65	1.6
PU-90%HS	1.45	0.57	40	0.94	65	1.7

and electron densities, respectively. If one assumes complete phase separation, the methodology employed to compute the theoretical electron densities of the soft and the hard phases can have a significant influence on the degree of phase separation extracted from the data. There are several factors that can significantly influence the values of the electron densities. One is the presence in the soft phase of so-called lone MDI units. They correspond to single MDI units which reacted during the synthesis with two soft segments and therefore are expected to reside in the soft phase and not to be part of the hard phase. Recently Garret et al. have investigated, using SAXS, a set of poly(urethane urea) block copolymers and calculated the theoretical electron density variances of the two phases, assuming complete phase separation, taking into account the presence of lone MDI units in the soft phase. It turns out that this correction is important mainly for low hard block content material.[10]

Another factor that can influence the electron densities of the phases are the degree of crytallinity. In our case, the soft segments are amorphous while the hard segments can crystallize. For MDI/BDO-based hard segments the reported densities of the amorphous and crystalline phases range from 1.25 to 1.58 g/cm^3 depending on the crystalline form.[23,24] In our previous work, some wide-angle X-ray scattering experiments where performed to examine hard block crystallinity. The presence of some ordered structures could be observed in the hard phase after annealing the samples for 72 h at 120 °C. Nevertheless the overall degree of crystallinity observed was very low.[8] We thus expect the density of the hard phase in our samples to be close to the density of the hard phase in the amorphous state.

Our previous work on the same set of samples suggested the presence in this system of almost "pure" soft and hard phases after 72 h annealing at 120 °C.[8] We opted therefore to compute electron densities based on a completely phase-separated model, where the soft phase corresponds to the soft segments and the hard phase to the hard segments. The electron density variance assuming complete phase separation can be calculated using the soft segment (SS) and hard segment (HS) volume fraction (Φ_{SS}, Φ_{HS}) and electron densities (ρ_{SS}, ρ_{HS}):

$$\overline{\Delta\rho_c^2} = \Phi_{HS}\Phi_{SS}(\rho_{HS} - \rho_{SS})^2 \tag{8}$$

For a polymer, knowing its mass density, ρ_m, the electron density, ρ_e, can be calculated from the molar mass, M_u, and the numbers of electrons, N_e, of its repeat unit through

$$\rho_e = \frac{N_{e^-}}{M_u} \times \rho_m \tag{9}$$

In our case, the repeat unit taken for the hard segment was a MDI−MP−diol unit and for the soft segment a PO unit. For the soft segments, the pure polyol density (1.02 g/cm^3) was used, and for the hard segment, the density measured for the amorphous PU-100%HS sample (1.27 g/cm^3) was used. It should be noted that the density obtained for our hard segment is in good agreement with the density reported in the literature for the amorphous MDI/BDO-based hard segments.[23,24] We obtained for our hard segment an electron density of $\rho_{HS} = 0.680$ e$^-$ mol/cm^3 and for the soft segment $\rho_{SS} = 0.563$ e$^-$ mol/cm^3. The calculated electron density variances assuming complete phase separation obtained for our samples are listed in Table 2.

The experimental electron density variance can be calculated for a two-phase system from the one-dimensional scattering data using the Porod invariant Q through[14,15,25,26]

$$\overline{\Delta\rho_e^2} = \frac{Q}{2\pi^2 i_e N_A^2} \tag{10}$$

i_e being Thompson's constant for the scattering from one electron (7.94×10^{-26} cm^2) and N_A Avogadro's number (6.02×10^{23} mol^{-1}). Q is defined as[14,15]

$$Q = \int_0^\infty \frac{[I(q) - I_b(q)]}{H(q)} q^2 \, dq \tag{11}$$

$I_b(q)$ being the background scattering due to thermal fluctuation and $H(q)$ is a function which models the size and shape of the interfacial boundary between the two phases. For a sigmoidal-shaped interface:

$$H(q) = \exp(-\sigma^2 q^2) \tag{12}$$

the thickness of the interface E being related to σ through

$$E \cong \sqrt{2\pi}\,\sigma \tag{13}$$

For a sharp interface $E = 0$, $H(q) = 1$ and

$$Q = \int_0^\infty [I(q) - I_b(q)] q^2 \, dq \tag{14}$$

The values of $I_b(q)$ and σ can be extracted from the scattering data using the Porod law which gives the scattering intensity of a two-phase system at high q values[14,15]

$$I(q) = \frac{K_p}{q^4} \exp(-\sigma^2 q^2) + I_b(q) \tag{15}$$

K_p being the Porod constant. In the investigated q range the background intensity, I_b, can be considered constant.

The values of K_p, σ, and I_b are then obtained by fitting the tail of the scattering curves.

It should be noted that the invariant calculation from the one-dimensional scattering patterns as described here is valid only for isotropic systems. As mentioned earlier, the high hard block content samples PU-80%HS and PU85%HS show some anisotropy, which results in the presence of a peak at low q values. Nevertheless due to the fact that the main peak is isotropic, suggesting that most of the sample is isotropic, and the fact that the invariant is calculated from $q^2I(q)$, the presence of the peak at low q should not have a significant influence on the values of the calculated invariant, at least for the PU-85%HS sample.

Before comparing the degree of phase separation of samples with different hard segment content, one must ensure that all samples are in the same or equivalent thermodynamic state. The thermodynamic investigation of this set of samples showed that the rate of phase separation is related to the hard segment content. In our case, it turns out that after 72 h of annealing at 120 °C the phase separation process has reached its maximum for all the samples.[8]

The experimental electron density variances and the degrees of phase separation obtained for our set of samples are listed in Table 2. The PU-50%HS sample seems to have a higher degree of phase separation compared to the other samples (see Table 2). As said earlier it is not clear whether this sample has the same structure/morphology as the higher hard block content samples. Nevertheless, the overall degree of phase separation calculation is still valid.

For the other samples, if a sharp interface model is considered, the overall degree of phase separation is found to be decreasing from 47% to 40% with increasing hard segment content, while if a sigmoidal interface model is considered then the overall degree of phase separation is found to be almost constant, ~65%, but the interface thickness is found to be increasing from 1.8 to 2.4 nm with increasing hard block content (Table 2). As already discussed by Koberstein et al. the sigmoidal shape is the most probable shape for the interface between the soft and the hard phases in polyurethanes block copolymers.[15,27]

The overall degree of phase separation obtained for our samples is relatively high compared to other polyurethane systems[10,13] suggesting a strong incompatibility between the soft and hard segments used in our system. This result is in good agreement with our previous results obtained by DSC also suggesting a strong phase separation in these materials.[8]

The fact that the same degree of phase separation is obtained for all the samples with a hard segment content higher than 65 wt % is in good agreement with the morphological interpretation made earlier. Indeed, as stated previously, the phase separation during the annealing process is expected to take place in the mixed phase (Figure 4). This mixed phase is thought to have the same composition for all our samples, i.e., 65 wt % of hard segments. Therefore, we expect the degrees of phase separation obtained for all of the samples to be similar.

It should be noted that for the PU-80%HS sample a lower degree of phase separation is obtained. As stated earlier, this sample presents areas with lamellar type structures, which are therefore anisotropic (Figure 6). The degree of phase separation calculated through the described procedure will then result in an apparent degree of phase separation lower than what would be obtained if the samples were completely isotropic.

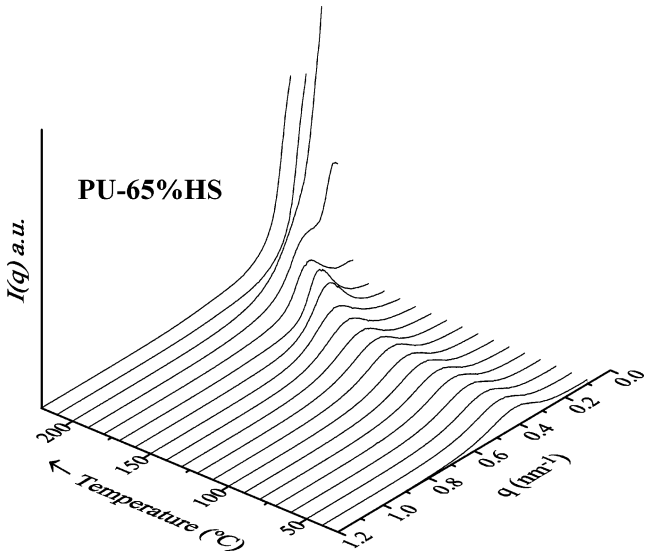

Figure 7. Intensity scattered by the PU-65%HS sample annealed beforehand for 72 h at 120 °C recorded during melting as a function of temperature.

Structure and Thermodynamics. In our previous work, we investigated the thermodynamic properties of the same set of samples as described here. From our results we assigned the melting endotherm observed at the higher temperature, T_{MMT}, to the microphase mixing transition of the soft and hard segments.[8] To give further support to this assignment, we performed the same type of melting and annealing experiments as performed using DSC, now in situ in the SAXS beam. The PU-65%HS and the PU-85%HS samples annealed beforehand for 72 h at 120 °C were used. First the samples were melted at 220 °C and then annealed at 120 °C, while the SAXS patterns were recorded as a function of temperature and time, respectively.

In Figure 7 are presented the scattering curves recorded during the melting of the PU-65%HS sample. As discussed earlier after 72 h annealing at 120 °C, the scattering curve shows a main scattering peak at $q^* = 0.43$ nm^{-1} characteristic of the microphase-separated morphology of the sample. Three stages in the melting process can be identified from Figure 7. Up to 120 °C, no significant changes are observed in the scattering curves. The position and the intensity of the scattering peak remain constant. After 120 °C, the peak position, q^*, shifts to smaller q values and its intensity increases. As already mentioned, 120 °C corresponds to the glass transition temperature of the hard segments. It is thus expected the mobility within the sample to increase significantly for temperatures higher than 120 °C. The increase in q^* suggests an increase in the size scale of the density fluctuations of the microphase-separated morphology. The role of annealing temperature on the structure and thermodynamic properties of this set of samples will be the subject of a forthcoming article.

A third stage occurs between 180 and 200 °C where the intensity of the scattering peak decreases and then disappears, indicating the occurrence of the microphase mixing of the soft and hard segments. The overall increase in the scattering intensity at low q is probably due to some foaming occurring within the sample due to the presence of moisture. Indeed, once the experiment

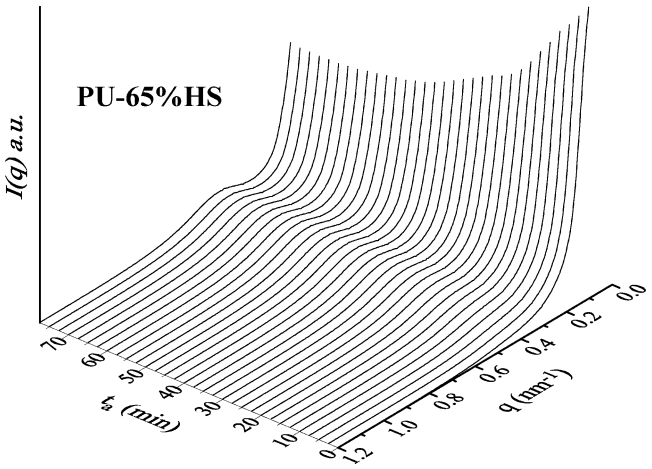

Figure 8. Intensity scattered by the PU-65%HS sample melted beforehand at 220 °C recorded during the annealing at 120 °C as a function of annealing time, t_a.

was finished, the sample was recovered and some bubbles could be observed. Nevertheless, the temperature range obtained for the microphase mixing of the soft and hard segments using SAXS is in very good agreement with the temperature, ~180 °C, obtained for the T_{MMT} transition using DSC.[8]

The same overall behavior was observed for the PU-85%HS sample. The main scattering peak, in this case too, is found to disappear between 180 and 200 °C. Here again a good agreement is found with our previous work, where the temperature of the T_{MMT} transition was found to be little dependent on the hard segment content of the samples.[8]

After melting, the samples were annealed at 120 °C. In Figure 8 are presented the scattering curves recorded as a function of the annealing time. From this figure it can be seen that the scattering peak is reappearing with increasing annealing time at the same position, $q^* = 0.43$ nm^{-1}, indicating that the sample is going through phase separation and that the same microphase-separated morphology is obtained. This suggests that the morphologies obtained for our samples correspond to a thermodynamic "stable" state, by melting and reannealing the sample the same morphology is obtained in a reproducible way. The position of the scattering peak is constant suggesting that the size scale of the density fluctuations remains constant during the phase separation process.

In Figure 9, the areas under the scattering peaks observed for the PU-65%HS and PU-85%HS samples are plotted as a function of annealing time. The intensity of the scattering peak increases, suggesting an increase in the degree of phase separation, up to a certain annealing time and then becomes constant. The same overall behavior is observed for the two samples, but the time scales involved are different.

For the PU-65%HS sample, the phase separation starts almost immediately and is at its maximum after 30−40 min while for the PU-85%HS sample a delay time of ~30 min is observed before the start of the phase separation process, and phase separation reaches its maximum after ~5 h. The results obtained for the dynamics of the phase separation in these two samples are in very good agreement with our previous results obtained using DSC. The same behavior was observed for the enthalpy variation of the T_{MMT} transition as a function of annealing time.[8] Our SAXS results seem to confirm the existence of a delay time for the start of the phase separation in the PU-85%HS sample. They also confirm the dependence of the phase separation rate on the hard segment content of the sample. A good agreement is obtained between our SAXS and DSC results for the time needed to reach the maximum of the phase separation for these two samples.

The overall dynamics of phase separation observed for our samples agrees well with what was observed for other block copolymers.[22,28−30] It is interesting to note that Hashimoto et al., for a polystyrene/polyisoprene diblock copolymer, also found the presence of a delay time (called "incubation time" by these authors) before the actual start of the phase separation process.[29] They also observed, following the delay time, an increase in the scattering peak intensity, the peak intensity becoming constant once the phase separation process reaches its maximum. These authors too observed no changes in the scattering peak position throughout the phase separation process.[29]

Finally a final SAXS experiment was performed using the PU-50%HS and a Linkam hot stage. In Figure 10, the scattering curves recorded during the remelting of a melt-quenched sample (i.e., melt at 220 °C followed by a room-temperature quench) are presented. In the graph inserted on the top left corner, the corresponding DSC curve obtained for the same sample is presented.[8] In our previous work, we assigned the exothermic transition (T_{MST}) to the microphase separation of the soft and hard segments and the endothermic transition (T_{MMT}) to the microphase mixing of the soft and hard segments. As can be seen in Figure 10, our SAXS results confirm this assignment. Indeed the peak in the scat-

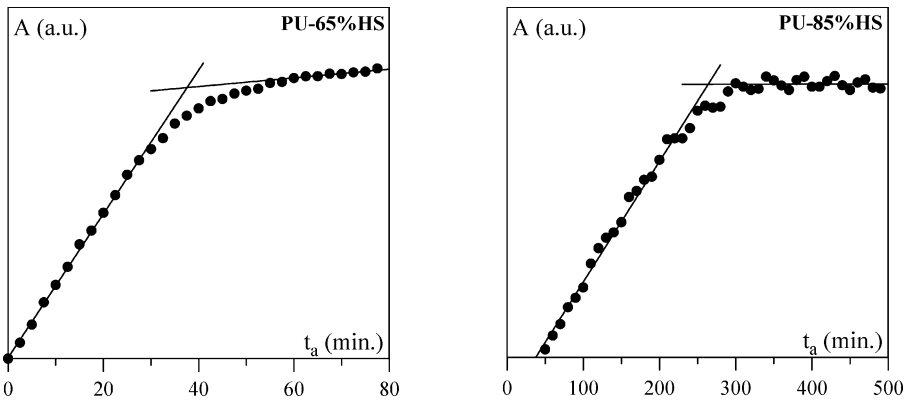

Figure 9. Area of the scattering intensity peak at $q_{max} = 0.43$ nm^{-1} as a function of annealing time, t_a, for the PU-65%HS (left) and the PU-85%HS (right) samples.

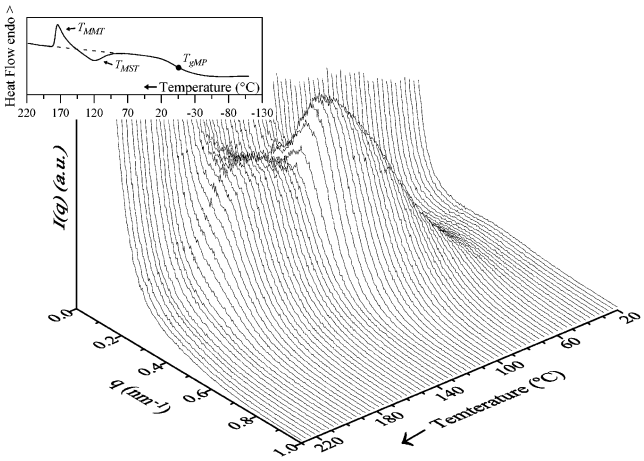

Figure 10. Intensity scattered by the PU-50%HS sample melted beforehand at 220 °C recorded during the following heating at 5 °C/min as a function of temperature. In the up-left corner the DSC thermograph obtained at 20 °C/min for the same sample is shown.

tering curve, characteristic of a microphase-separated state, is seen to be appearing between 60 and 130 °C and then disappearing between 130 and 200 °C. The temperature ranges in which the two phenomena are observed are in good agreement with DSC thermograph bearing in mind that the two experiments have been done at different heating rates.

All these experiments clearly show the correlation existing between the so-called T_{MMT} transition and the presence in the scattering curve of an intensity maximum characteristic of a microphase-separated system. These results give further support to the assignment of the T_{MMT} melting endotherm to the microphase mixing of the soft and hard segments.

Conclusion

The structure and morphology of a set of high hard block content TPUs have been investigated using mainly SAXS and TEM. The results of this investigation have been correlated with thermodynamic properties measured previously.[8] The investigation of the dynamics of the phase separation clearly demonstrated a strong correlation between the SAXS intensity peak at 0.43 nm^{-1} and the melting enthalpy of the so-called T_{MMT} transition, providing further support to the assignment made (from our previous work[8]) of this endotherm to the microphase mixing of the soft and hard segments. The SAXS experiment also showed that the rate of phase separation is a function of the hard segment content of the sample. For the high hard segment content sample a delay time before the start of phase separation has been identified as well. These results are in very good agreement with the results obtained from the thermodynamic investigation of this set of samples.

Samples with hard segment contents higher than 65 wt % were shown to have a continuous hard phase matrix in which soft phase domains are embedded. The estimated average interdomain distance extracted from the scattering curves ($d_i \approx 15$ nm) was found to be the same for all the samples. Reinforced by the previous DSC measurements,[8] these results suggest that the melt-quenched samples have a two phase structure: a "pure" hard segment phase + a mixed phase (soft + hard segments with a hard segment content of 65 wt %). The mixed phase undergoes further phase separation during the annealing process resulting in the same interdomain distance for all the samples. The overall scattering intensities were found to decrease linearly with decreasing soft segment volume fraction, giving further support to this interpretation.

Alignment of the soft phase domains was observed in some samples, resulting in a lamellar type morphology. The inter lamellar repeat distance, d_l, is found to increase with increasing hard segment content. The alignment of the soft phase domains responds to and is determined by the preparation method used.

The same degree of phase separation was found for all the samples with hard segment content higher than 65 wt % when a sigmoidal interface was chosen between hard and soft domains. The interface thickness was found to increase with increasing hard segment.

Acknowledgment. The authors gratefully acknowledge ICI plc for their financial support from their strategic research fund, CRG D2AM for the use of beamline BM02 at ESRF, H. Verbeke from Huntsman Polyurethanes for the synthesis of the samples, Dr. J. P. A. Fairclough from Sheffield University, Sheffield, U.K., for his support in the use of beamline 8.2 (CCLRC), and Prof. C. B. Bucknall and P. Logan from Cranfield University, Cranfield, U.K., for their support with the use of the TEM.

References and Notes

(1) *Polyurethanes Handbook*; Hanser: Munich, Germany, 1994.
(2) Woods, G. *The ICI Polyurethanes Book*, 2nd ed.; John Wiley and Sons: New York, 1990.
(3) Voronov, V. P.; Buleiko, V. M.; Podneks, V. E.; Hamley, I. W.; Fairclough, J. P. A.; Ryan, A. J.; Mai, S.-M.; Liao, B.-X.; Booth, C. *Macromolecules* **1997**, *30*, 6674−6676.
(4) Chen, T. K.; Shieh, T. S.; Chui, J. Y. *Macromolecules* **1998**, *31*, 1312−1320.
(5) Frontini, M. F.; Pavan, A. *J. Appl. Polym. Sci.* **1993**, *48*, 2003−2022.
(6) Koberstein, J. T.; Galambos, A. F. *Macromolecules* **1992**, *25*, 5618−5624.
(7) Phillips, R. A.; Cooper, S. L. *J. Polym. Sci., Part B: Polym. Phys.* **1996**, *34*, 737−749.
(8) Saiani, A.; Daunch, W. A.; Verbeke, H.; Leenslag, J.-W.; Higgins, J. S. *Macromolecules* **2001**, *34*, 9059−9068.
(9) Li, Y.; Ren, Z.; Zhao, M.; Yang, H.; Chu, B. *Macromolecules* **1993**, *26*, 612−622.
(10) Garrett, J. T.; Runt, J.; Lin, J. S. *Macromolecules* **2000**, *33*, 6353−6359.
(11) Chu, B.; Gao, T.; Li, Y.; Wang, J.; Desper, C. R.; Byrne, C. A. *Macromolecules* **1992**, *25*, 5724−5729.
(12) Ryan, A. J.; Macosko, C. W.; Bras, W. *Macromolecules* **1992**, *25*, 6277−6283.
(13) Koberstein, J. T.; Galambos, A. F.; Leung, L. M. *Macromolecules* **1992**, *25*, 6195−6204.
(14) Roe, R.-J. *Methods of X-ray and Neutron Scattering in Polymer Science*; Oxford University Press: New York, 2000.
(15) Leung, L. M.; Koberstein, J. T. *J. Polym. Sci., Part B: Polym. Phys.* **1985**, *23*, 1883−1913.
(16) Guinier, A.; Fournet, G. *Small-Angle Scattering of X-rays*; John Wiley & Sons: New York, 1955.
(17) Garrett, J. T.; Lin, J. S.; Runt, J. *Macromolecules* **2002**, *35*, 161−168.
(18) Li, C.; Goodman, S. L.; Albrecht, R. M.; Cooper, S. L. *Macromolecules* **1988**, *21*, 2367−2375.
(19) Chentsai, C. H. Y.; Thomas, E. L.; Macknight, W. J.; Schneider, N. S. *Polymer* **1986**, *27*, 659−666.
(20) Serrano, M.; Macknight, W. J.; Thomas, E. L.; Ottino, J. M. *Polymer* **1987**, *28*, 1667−1673.
(21) Garrett, J. T.; Siedlecki, C. A.; Runt, J. *Macromolecules* **2001**, *34*, 7066−7070.
(22) Hamley, I. W. *The Physics of Block Copolymers*; Oxford University Press: Oxford, U.K., 1998.
(23) Blackwell, J.; Lee, C. D. *J. Polym. Sci.: Polym. Phys. Ed.* **1984**, *22*, 759−772.

(24) Briber, R. M.; Thomas, E. L. *J. Polym. Sci.: Polym. Phys. Ed.* **1985**, *23*, 1915−1932.
(25) Ruland, W. *J. Appl. Crystallogr.* **1971**, *4*, 70−73.
(26) Bonart, R.; Müller, E. H. *J. Macromol. Sci. Phys.* **1974**, *B10* (1), 177−189.
(27) Koberstein, J. T.; Leung, L. M. *Macromolecules* **1992**, *25*, 6205−6213.
(28) Stühn, B.; Vilesov, A.; Zachmann, H. G. *Macromolecules* **1994**, *27*, 3560−3565.
(29) Hashimoto, T.; Sakamoto, N. *Macromolecules* **1995**, *28*, 4779−4781.
(30) Li, Y.; Gao, T.; Chu, B. *Macromolecules* **1992**, *25*, 1737−1742.

MA034604+